SYSTEM-LEVEL THERMAL OPTIMIZATION OF FORCED-AIR COOLING FOR COMPACT HIGH-POWER ELECTRONIC SYSTEMS: APPLICATION TO A GAN MMIC AMPLIFIER

Ali Jebelli [1,*], Nafiseh Lotfi [2], Arezoo Mahabadi [3], and Mustapha C. E. Yagoub [4]

[*1] College of Business, Engineering, and Technology, Kentucky State University, Kentucky, USA

[2] Department of Engineering and Design, Robotic Century, Kansas, USA

[3] Department of Engineering and Design, Robotic Century, Alberta, Canada

[4]School of Electrical Engineering and Computer Science, University of Ottawa, Ontario, Canada

***** Corresponding author; E-mail: ali.jebelli@kysu.edu

Efficient thermal management is essential in compact high-power electronic systems, where elevated operating temperatures can degrade performance and reduce operational reliability. This study presents a system-level thermal optimization of forced-air cooling for a compact high-power electronic amplifier with high thermal loading. The objective is to improve cooling effectiveness through the structured optimization of practical thermal management parameters without introducing a new cooling technology.

A numerical methodology based on conjugate heat transfer simulations is used to evaluate the influence of fan performance, airflow orientation, enclosure airflow organization, and passive heat-sink integration under identical operating and geometric conditions. The thermal effect of each modification is examined sequentially to identify the most effective cooling configuration.

The results show that airflow organization strongly influences thermal behavior, and that lateral airflow improves convective heat removal and temperature uniformity compared with the baseline vertical airflow configuration. The addition of a compact finned copper heat sink further enhances heat spreading and cooling performance. The best-performing investigated configuration reduces the maximum device surface temperature from approximately 50 °C to 35 °C under identical operating conditions.

The proposed methodology provides practical design guidance for the thermal optimization of compact high-power electronic systems and can be extended to similar forced-air cooling applications.

Keywords: thermal management; forced-air cooling; electronic cooling; heat transfer; conjugate heat transfer; numerical simulation; heat sink optimization; compact electronic systems; thermal design; cooling performance

1. Introduction

High-power radio-frequency (RF) and microwave systems increasingly rely on Gallium Nitride (GaN)-based Monolithic Microwave Integrated Circuits (MMICs) because of their high breakdown voltage, superior power density, and excellent performance at microwave and millimeter-wave frequencies [1–3,14]. However, the same properties that enable high output power also generate substantial heat within highly compact device footprints, creating severe thermal management challenges. If this heat is not effectively dissipated, elevated operating temperature can degrade amplifier efficiency, reduce gain stability, accelerate material degradation, and shorten device lifetime [4,5].

Although GaN devices are commonly fabricated on silicon carbide (SiC) substrates with relatively high thermal conductivity, substrate-level heat spreading alone is often insufficient under sustained high-power operation [4]. The thermal behavior of GaN MMICs is closely linked to key reliability indicators such as mean time to failure (MTTF), threshold voltage drift, and long-term performance stability [5]. Excessive temperature can also significantly affect reliability in compact high-power electronic systems more broadly [9]. Consequently, thermal management has become a major system-level design constraint in compact high-power RF electronics, often limiting achievable performance and reliability more than the intrinsic electrical capability of the device itself. Recent studies have further emphasized the relationship between operating conditions, efficiency, and reliability in high-power microwave amplifier systems [20].

A wide range of thermal management approaches has been investigated for GaN-based power devices. Passive methods such as improved substrate materials, thermal vias, and backside metallization can enhance conductive heat spreading from the active region [4]. More advanced cooling strategies, including liquid cooling, microchannel cooling, and hybrid active-passive solutions, have demonstrated strong heat-removal performance in high heat-flux applications [6–10]. However, these approaches often introduce fabrication complexity, increased cost, packaging challenges, and integration constraints that limit their practicality for many commercial RF and microwave modules [10–13]. Similarly, advanced packaging technologies such as low-temperature co-fired ceramic (LTCC) and fan-out packaging may improve thermal performance, but they can also introduce electromagnetic parasitics and manufacturing limitations, especially at high operating frequencies [11,12].

In contrast, forced-air cooling combined with passive heat-spreading structures remains one of the most practical, scalable, and cost-effective thermal management solutions for compact commercial GaN MMIC amplifiers [7,8]. Despite its widespread use, the thermal performance of forced-air cooling systems is highly sensitive to airflow organization, fan characteristics, enclosure geometry, and heat-sink configuration [6–8]. Prior studies have shown that airflow path design and passive thermal structures can strongly influence convective heat transfer effectiveness and temperature uniformity in compact electronic systems [21]. Nevertheless, much of the existing literature remains focused on isolated cooling components, such as stand-alone heat sinks, simplified fan arrangements, or idealized airflow domains, rather than on the integrated optimization of the full cooling architecture under realistic enclosure-level constraints.

Moreover, although commercial multiphysics tools such as ANSYS Fluent and ANSYS Icepak are widely used for electronics cooling analysis, the optimization methodology itself is often insufficiently documented in the open literature. As a result, many published studies provide isolated thermal results without offering a reproducible design framework that can be generalized to practical RF amplifier systems.

This creates a gap between detailed numerical simulation and application-oriented thermal design guidance for compact high-power GaN MMIC modules.

To address this gap, this work presents a system-level thermal optimization framework for the forced-air cooling of a commercial high-power GaN MMIC amplifier (QPA1010). Rather than introducing a new cooling technology, the study focuses on the structured optimization of practical thermal management parameters, including fan performance, airflow orientation, enclosure flow organization, and passive heat-sink integration, under fixed power dissipation and geometric constraints. A sequential parametric simulation strategy is employed using conjugate heat transfer modeling in ANSYS Fluent and ANSYS Icepak to evaluate the thermal impact of each design modification in a transparent and reproducible manner.

The contribution of this work lies in establishing a practical engineering optimization methodology that bridges the gap between detailed numerical thermal analysis and scalable cooling design for compact RF electronics. The proposed approach enables quantitative comparison of competing cooling configurations and provides actionable design guidance for improving the thermal performance and reliability of GaN MMIC amplifier systems where experimental prototyping or advanced cooling technologies may be impractical.

2. Theoretical Background and Governing Equations

2.1. Heat Transfer Mechanisms

The thermal behavior of high-power GaN MMIC amplifiers is governed by the coupled interaction of heat conduction within solid materials and forced convection in the surrounding airflow. Accurate prediction of the temperature distribution therefore requires a conjugate heat transfer (CHT) formulation, in which heat transfer in the solid and fluid domains is solved simultaneously. This approach is widely used in the thermal analysis of electronic packages, RF power modules, and compact electronic cooling systems because it captures realistic heat-flow paths and fluid–solid thermal interactions [8,15–18].

Three modes of heat transfer may be present in compact electronic cooling systems: conduction, convection, and radiation [15,17]. In the present study, conduction governs heat transport within the GaN MMIC, PCB, copper heat spreader, heat sink, and enclosure materials. Forced convection is the dominant mechanism for heat removal from exposed surfaces due to airflow generated by axial fans. Thermal radiation is neglected because its contribution is small compared with forced convection under the investigated temperature range and airflow conditions, which is a common assumption in forced-air cooling analyses of compact electronic systems [8,15,17].

Accordingly, the governing formulation includes heat conduction in the solid regions and forced convection with energy transport in the fluid domain.

2.2. Governing Equations for Fluid Flow

Airflow inside the enclosure is modeled as a steady-state, incompressible Newtonian fluid. Under these assumptions, the governing equations for mass and momentum conservation are expressed as follows [16,18].

Continuity equation:

$$\nabla \cdot u = 0 \qquad (1)$$

where **u**is the fluid velocity vector.

Momentum equation:

$$\rho(u \cdot \nabla)u = -\nabla p + \nabla \cdot \left[\mu_{eff}(\nabla u + \nabla u^T)\right] \qquad (2)$$

where ρ is the fluid density, p is the pressure, and μ_{eff} is the effective dynamic viscosity of air.

Although Eq. (2) is written in the incompressible momentum-conservation form, this does not imply that the airflow is restricted to purely laminar behavior. In compact forced-air electronic enclosures, fan-driven airflow may produce local acceleration, separation, recirculation, and transitional or turbulent flow behavior [8,16,18,21]. Therefore, the momentum equation is expressed using an effective viscosity, μ_{eff}, which may include both molecular viscosity and additional effective-viscosity contributions associated with the numerical flow model. This formulation is suitable for representing forced-air cooling behavior in compact enclosures. The same flow-modeling approach and solver settings were applied consistently to all investigated cooling configurations so that the relative comparison among the baseline, fan-enhanced, airflow-reoriented, and heat-sink-integrated cases remains valid.

These equations govern the airflow behavior inside the enclosure and determine the velocity field that influences convective heat transfer from the thermally active surfaces.

2.3. Energy Equation and Heat Conduction

The thermal temperature field is obtained by solving the energy equation in the fluid domain together with the heat conduction equation in the solid regions [15–18].

Energy equation in the fluid domain:

$$\rho c_p(u \cdot \nabla T) = \nabla \cdot (k_f \nabla T) \qquad (3)$$

where T is temperature, c_p is the specific heat capacity of air, and k_f is the thermal conductivity of the fluid.

Heat conduction equation in solid regions:

$$\nabla \cdot (k_s \nabla T) + \dot{q} = 0 \qquad (4)$$

where $k_s$is the thermal conductivity of the solid material and $\dot{q}$represents the volumetric heat generation within the solid region.

In the present study, the GaN MMIC is modeled as the primary heat-generating region, with the applied heat load corresponding to the specified device power dissipation. The heat generated in the MMIC is conducted through the device structure, copper heat spreader, PCB, heat sink when present, and enclosure, and is subsequently removed by forced airflow inside the enclosure. This coupled solid–fluid treatment is consistent with standard CHT modeling practice for compact electronic packages and power devices [8,15–19].

2.4. Convective Heat Transfer and Conjugate Interface Conditions

Convective heat transfer between solid surfaces and airflow can be described in simplified form by Newton's law of cooling [15,17]:

$$Q_{conv} = hA_s(T_s - T_\infty) \qquad (5)$$

where Q_{conv} is the convective heat-transfer rate, $h$is the convective heat-transfer coefficient, A_s is the exposed heat-transfer area, T_s is the surface temperature, and T_∞ is the bulk air temperature.

In the present work, the convective heat-transfer coefficient is not prescribed directly. Instead, it emerges from the numerical solution of the coupled momentum and energy equations and depends on airflow velocity, flow organization, local recirculation, surface exposure, and heat-sink geometry [16,18]. Consequently, changes in fan performance, airflow orientation, and heat-sink configuration directly influence thermal performance by modifying the effective convective heat-transfer behavior [8,21].

For the conjugate heat-transfer formulation, temperature continuity and heat-flux continuity are imposed at each solid–fluid interface [15–18]. These interface boundary conditions are expressed as:

$$T_s = T_f \quad (6)$$

$$-k_s \frac{\partial T_s}{\partial n_s} = -k_f \frac{\partial T_f}{\partial n_f} \quad (7)$$

where T_s and T_f are the solid-side and fluid-side interface temperatures, respectively; k_s and k_f are the thermal conductivities of the solid and fluid domains; and n_s and n_f are the corresponding normal directions at the interface. These conditions ensure that heat conducted through the solid components is transferred consistently to the airflow without prescribing an empirical heat-transfer coefficient at the interface.

2.5. Modeling Assumptions

To ensure computational efficiency while preserving the dominant physical behavior of the cooling system, the following assumptions are adopted:

1. Steady-state operation is considered.
2. Air is treated as an incompressible Newtonian fluid.
3. Thermophysical properties are assumed to be constant over the investigated temperature range.
4. Solid materials are assumed to be homogeneous and isotropic.
5. Perfect thermal contact is assumed at bonded solid–solid interfaces.
6. Heat generation within the MMIC active region is modeled as uniformly distributed.
7. Thermal radiation is neglected because forced convection is the dominant heat-removal mechanism under the investigated conditions.
8. The same numerical modeling assumptions and solver settings are applied to all configurations to ensure a consistent comparative assessment.

These assumptions are consistent with established practices in CFD-based thermal analysis of compact forced-air electronic cooling systems [8,15–18,21].

2.6. Summary of Theoretical Framework

The theoretical framework presented in this section establishes the physical basis for the numerical simulations and optimization methodology described in the subsequent sections. By employing a conjugate heat-transfer formulation that couples fluid flow, solid conduction, and solid–fluid interface heat transfer,

the model captures the dominant heat-transfer mechanisms governing the thermal behavior of the GaN MMIC amplifier under forced-air cooling conditions [15–18].

The revised formulation also clarifies that the momentum equation is not intended to imply a purely laminar-flow-only model. Instead, the airflow field is represented using a forced-flow numerical formulation suitable for compact electronic enclosures, where recirculation and nonuniform velocity distributions may occur [8,16,18,21]. This provides a consistent basis for evaluating the relative thermal performance of different fan, airflow, and heat-sink configurations.

3. System Description and Numerical Methodology

3.1. Physical Configuration of the Cooling System

The investigated system is based on a compact high-power GaN MMIC amplifier mounted on a printed circuit board (PCB) and enclosed within a metallic housing. The MMIC has overall package dimensions of 4.5 mm × 5.0 mm × 1.72 mm [22], the MMIC is treated as the primary heat-generating component, while the surrounding PCB, copper heat spreader, heat sink, and enclosure provide conduction and convection paths for heat removal.

The device is mounted on the PCB through a thin metallic bonding/interface layer to provide mechanical support and thermal conduction. A copper base plate is positioned beneath the MMIC and acts as the primary heat spreader, while the surrounding aluminum enclosure provides mechanical support and an auxiliary heat-spreading path. Forced-air cooling is applied using fan-driven airflow through the enclosure, creating an internal airflow path for convective heat removal.

In the final investigated configuration, a compact finned copper heat sink is integrated into the airflow path to increase the effective heat-transfer area and improve air–solid thermal interaction. To ensure a consistent basis for comparison, the device geometry, enclosure dimensions, material properties, applied heat load, ambient condition, and numerical settings are maintained constant throughout all investigated configurations. Only the selected cooling-design parameter, such as fan capacity, airflow orientation, or heat-sink integration, is modified at each optimization stage.

Fig. 1 shows the amplifier power board with the GaN MMIC centrally mounted on the heat-dissipating assembly within the enclosure. Fig. 2 presents the schematic cooling configuration, including the GaN MMIC, copper heat spreader, PCB layer, and aluminum enclosure considered in the numerical model.

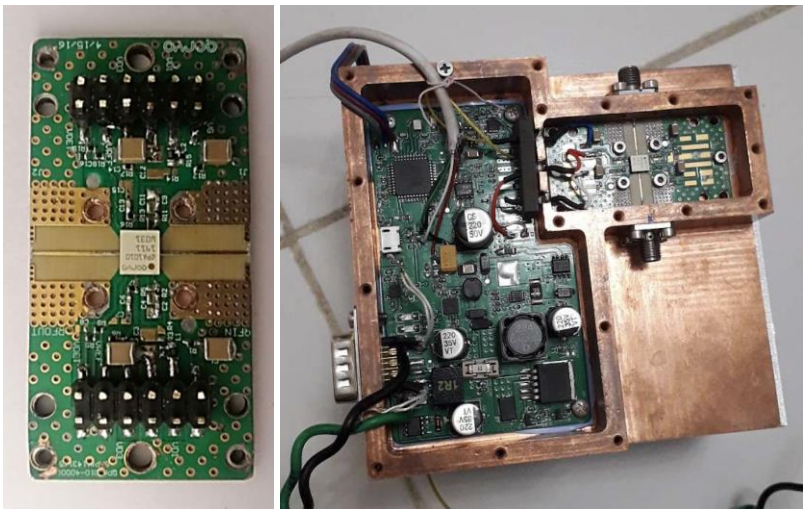

Fig 1. Amplifier power board with centrally mounted QPA1010 GaN MMIC.

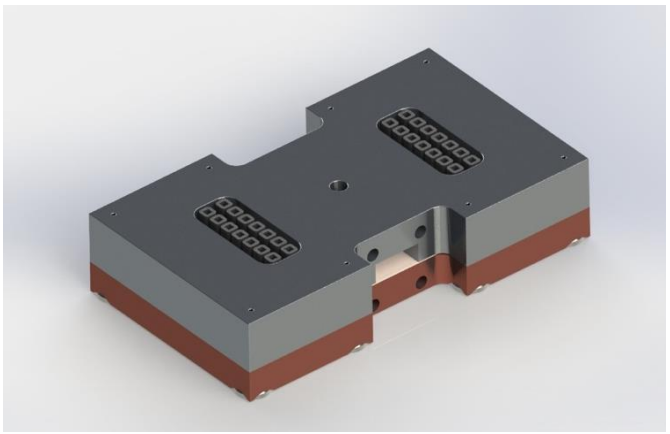

Fig 2. Schematic of the cooling configuration showing the GaN MMIC, copper heat spreader, PCB, and aluminum enclosure.

3.2. Material Properties

All solid materials in the numerical model are assumed to be homogeneous and isotropic, with constant thermophysical properties evaluated at room temperature. Air is modeled as an incompressible fluid with constant properties. The temperature dependence of material properties is neglected because the investigated operating range is sufficiently narrow for comparative system-level thermal analysis. This assumption is commonly adopted in CFD-based electronics cooling studies where the primary objective is to compare relative thermal trends among design configurations [15–18].

The materials used in the numerical model include GaN for the active device, copper C110 for the heat spreader and heat sink, aluminum 6061-T6 for the enclosure, Rogers dielectric material for the PCB substrate, and air as the cooling fluid. The corresponding thermophysical properties adopted in the simulations are summarized in Tab. 1.

Table 1. Thermophysical properties of materials used in the numerical model

Component	Material	Thermal Conductivity (W/m·K)	Specific Heat (J/kg·K)	Density (kg/m³)
MMIC	Gallium Nitride (GaN)	130	490	6070
Heat spreader / Heat sink	Copper C110	401	385	8933
Enclosure	Aluminum 6061-T6	167	896	2700
PCB	Rogers dielectric	1.03	—	2300
Cooling fluid	Air	0.026	1007	1.225

3.3. Computational Domain and Boundary Conditions

A full three-dimensional conjugate heat-transfer computational domain is constructed to include the GaN MMIC, PCB, copper base/spreader, aluminum enclosure, heat sink when applicable, and the surrounding internal airflow region. The purpose of the computational domain is to capture the coupled interaction between heat conduction in the solid components and forced convection within the enclosure airflow path.

The MMIC is modeled as a volumetric heat source corresponding to the specified device thermal load used consistently throughout all simulations. The heat generation is uniformly distributed within the active device region. Ambient air enters the enclosure through the fan-driven inlet boundary, while a pressure outlet condition is imposed at the designated exhaust opening. The same inlet air temperature, applied heat load, enclosure dimensions, material properties, and numerical settings are maintained for all investigated configurations to ensure a consistent comparative assessment.

All external enclosure walls are assumed to be thermally insulated except where heat exchange with the internal airflow is explicitly resolved through the conjugate heat-transfer formulation. At all solid–fluid interfaces, continuity of temperature and heat flux is imposed so that heat conducted through the solid regions is transferred consistently to the airflow. Perfect thermal contact is assumed at bonded solid–solid interfaces, including the MMIC-to-base and base-to-enclosure connections. This assumption is appropriate for the present comparative optimization study because the main objective is to evaluate relative thermal-performance trends across different cooling configurations.

The fan/inlet and outlet locations are modified according to the investigated cooling configuration. In the baseline and fan-performance enhancement cases, the airflow is introduced in the vertical direction toward the internal heat-dissipating assembly. In the airflow re-orientation case, the inlet and outlet arrangement is modified to generate lateral airflow across the MMIC and copper heat spreader. In the final heat-sink-integrated configuration, the lateral airflow path is combined with a compact finned copper heat sink so that the airflow passes through or across the fin passages.

Fig. 3 illustrates the computational domain and applied boundary conditions used in the conjugate heat-transfer simulations, including the airflow inlet, outlet, and solid regions within the enclosure. The same boundary-condition framework is used throughout the study, while only the selected cooling-design parameter, such as fan capacity, airflow direction, or heat-sink integration, is changed at each optimization stage.

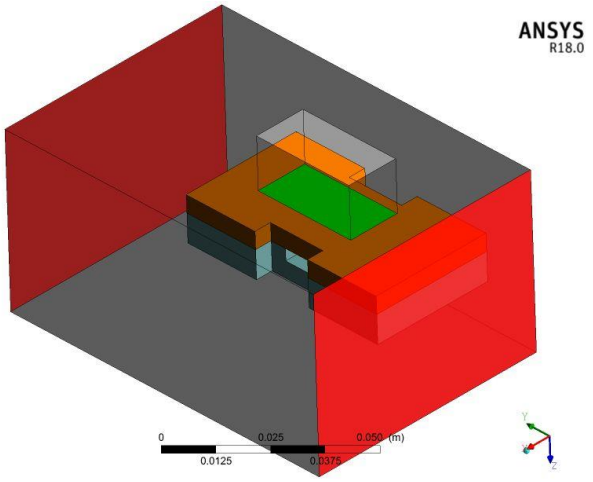

Fig 3. Computational domain and applied boundary conditions for the conjugate heat transfer model.

3.4. Governing Model and Solver Settings

The simulations are performed using ANSYS Fluent and ANSYS Icepak under steady-state conjugate heat-transfer conditions. Airflow within the enclosure is modeled as three-dimensional incompressible forced flow, and the thermal field is obtained by solving the coupled continuity, momentum, and energy equations in the fluid domain together with the heat-conduction equation in the solid regions.

Forced convection is not imposed using a prescribed heat-transfer coefficient. Instead, the local convective behavior emerges from the coupled numerical solution and depends on airflow velocity, airflow direction, local recirculation, surface exposure, and heat-sink geometry. This approach enables realistic evaluation of the influence of fan performance, airflow orientation, and passive heat-sink integration on the cooling behavior of the amplifier module.

The governing equations are discretized using the finite volume method. Pressure–velocity coupling is handled using the SIMPLE algorithm, and second-order spatial discretization is used for the momentum and energy equations to improve numerical accuracy. Convergence is assessed based on residual reduction and stabilization of the maximum MMIC surface temperature.

Because the investigated configurations involve fan-driven airflow in a compact enclosure, the flow may include local acceleration, recirculation, and transitional or turbulent behavior. Therefore, the numerical formulation is interpreted as a forced-airflow model suitable for compact electronics cooling, rather than as a purely laminar-flow-only model. The same flow-modeling approach, discretization scheme, and convergence criteria are used for all configurations to ensure that the comparison among design cases remains consistent.

Thermal radiation is neglected because its contribution is expected to be small compared with forced convection under the investigated temperature range and airflow conditions, which is a common assumption in compact forced-air electronics cooling simulations [15,17].

3.5. Mesh Generation and Grid Independence

A hybrid structured/unstructured mesh is generated for the conjugate heat-transfer domain. Local mesh refinement is applied in thermally and hydrodynamically critical regions, including the GaN MMIC, copper base plate, solid–fluid interfaces, fan inlet and outlet regions, and heat-sink fin channels when present. Special attention is given to resolving temperature gradients near the MMIC and airflow development within the enclosure.

Fig. 4 presents the computational mesh and mesh-quality assessment used in the numerical simulations. Fig. 4(a) shows the element-quality distribution, which evaluates the regularity of the mesh elements. Values closer to unity indicate more regular and numerically favorable elements. Fig. 4(b) shows the skewness distribution, which measures the deviation of mesh elements from an ideal shape. Lower skewness values indicate better mesh quality. Therefore, although both plots use element count on the vertical axis, the horizontal axes represent different mesh-quality indicators: element quality in Fig. 4(a) and skewness in Fig. 4(b). Fig. 4(c) shows the three-dimensional mesh structure used for the computational domain.

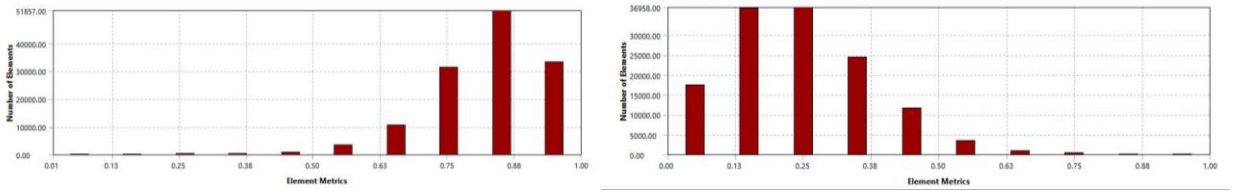

(a) (b)

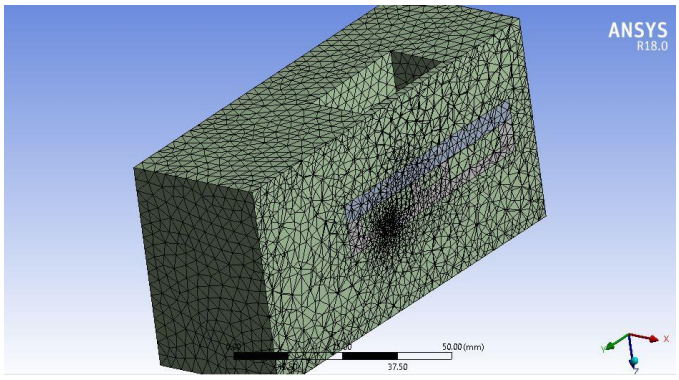

(c)

Fig 4. Computational mesh and mesh-quality assessment for the numerical model: (a) element-quality distribution, where values closer to 1 indicate better element quality; (b) skewness distribution, where lower values indicate better element shape; and (c) three-dimensional mesh structure.

To ensure numerical reliability, a grid-independence study is conducted using three progressively refined mesh densities. The maximum MMIC surface temperature is selected as the primary comparison metric because it directly reflects the thermal-performance objective of the study. As summarized in Tab. 2, the variation in predicted peak temperature between the medium and fine mesh cases remains below 1%, indicating that the numerical solution is sufficiently insensitive to further mesh refinement. Therefore, the

medium mesh is adopted for the subsequent simulations as a compromise between computational efficiency and numerical accuracy.

Table 2. Mesh-independence study for the baseline configuration

Mesh Level	Number of Cells	Max Temperature (°C)	Difference (%)
Coarse	846,320	50.8	—
Medium	1,347,580	50.2	1.18
Fine	2,108,940	49.9	0.60

3.6. Cooling Configurations and Optimization Procedure

The thermal optimization is conducted using a sequential parametric design strategy. Each cooling configuration is evaluated independently while maintaining the same heat load, enclosure dimensions, material properties, ambient temperature, and numerical solver settings. This stepwise methodology allows the thermal effect of each design modification to be isolated and compared systematically.

The term “optimized configuration” in this study refers to the best-performing configuration among the investigated sequential design modifications, rather than to a global mathematical optimization over all possible fan locations, fan capacities, and airflow paths. This clarification is important because the objective of the present work is to provide a practical engineering optimization framework based on representative cooling configurations.

The investigated configurations are summarized in Tab. 3.

Table 3. Summary of fan position and airflow organization for the investigated cooling configurations

Configuration	Fan/Inlet Position	Airflow Direction	Main Purpose of Case	Design Change Compared with Previous Case
Baseline configuration	Vertical/top inlet	Vertical airflow directed toward the internal heat-dissipating assembly	Reference cooling case	Original airflow arrangement
Fan-performance enhancement	Same position as baseline	Same vertical airflow direction as baseline	Evaluate effect of increased fan capacity	Airflow capacity increased; geometry and airflow direction unchanged
Airflow re-orientation	Lateral side inlet	Lateral cross-flow across MMIC and copper heat spreader	Reduce stagnant zones and improve airflow interaction with hot regions	Inlet/outlet arrangement modified to create lateral flow
Heat-sink-integrated optimized configuration	Lateral inlet with organized air channel	Lateral airflow through/across heat-sink fins	Increase convective area and improve heat spreading	Finned copper heat sink added to lateral airflow path

Tab. 3 clarifies the fan/inlet position and airflow organization used in each cooling configuration. In the baseline configuration, the fan-driven inlet introduces airflow vertically toward the internal heat-dissipating assembly. In the fan-performance enhancement case, the fan location and airflow direction remain the same as in the baseline configuration, while only the airflow capacity is increased. Therefore, this case isolates the effect of fan-capacity enhancement without changing the enclosure geometry or airflow path.

In the airflow re-orientation case, the inlet and outlet arrangement is modified to generate lateral cross-flow across the MMIC and copper heat spreader. This configuration is intended to improve airflow

interaction with the thermally critical region and reduce local recirculation or stagnant zones. In the final heat-sink-integrated configuration, the lateral airflow arrangement is combined with a compact finned copper heat sink and an organized air channel so that airflow passes through or across the fin passages.

The final configuration is selected because it produces the lowest maximum MMIC surface temperature and the greatest thermal-performance improvement among the investigated cases. Therefore, the optimization process is based on sequential comparison of practical engineering design modifications: fan-capacity increase, airflow-path reorientation, and heat-sink integration.

3.7. Fan and Airflow Configuration Description

To clarify the operational difference between the baseline and fan-performance enhancement cases, both cases use the same fan/inlet position and the same vertical airflow direction. The only difference is the prescribed airflow capacity. Therefore, the fan-performance enhancement case represents the use of a higher-capacity fan or an equivalent increase in inlet airflow rate relative to the baseline case.

In the present comparative study, the fan-performance enhancement is treated as a relative increase in fan capacity compared with the baseline condition, rather than as the characterization of a specific commercial fan model. This approach allows the influence of increased airflow capacity to be separated from the influence of airflow-path reorientation and heat-sink integration.

In the airflow re-orientation case, the airflow path is modified from vertical impingement-type flow to lateral cross-flow across the heat-dissipating components. This change is intended to increase the interaction between the airflow and the thermally active surfaces, while reducing local recirculation zones inside the enclosure.

In the final heat-sink-integrated configuration, the lateral airflow path is further organized using a compact finned copper heat sink and air-channel arrangement. This configuration increases the effective surface area exposed to airflow and promotes more uniform heat removal from the MMIC and copper heat spreader.

3.8. Evaluation Metrics

To enable consistent comparison among configurations, each case is evaluated using the following thermal and flow-performance indicators:

- maximum MMIC surface temperature;
- temperature distribution across the heat spreader and enclosure;
- airflow structure and streamline behavior;
- temperature uniformity within the cooling assembly;
- estimated thermal resistance.

The thermal-performance improvement of each configuration is quantified relative to the baseline case using:

$$Improvement(\%) = \frac{T_{max,baseline} - T_{max,case}}{T_{max,baseline}} \times 100 \qquad (8)$$

where $T_{\mathrm{max,baseline}}$ is the maximum MMIC surface temperature of the baseline configuration and $T_{\mathrm{max,case}}$ is the corresponding value for the modified configuration.

The thermal resistance of each configuration is estimated as:

$$R_{th} = \frac{T_{max} - T_{\infty}}{Q} \qquad (9)$$

where $T_{\max}$ is the maximum device surface temperature, T_{∞} is the ambient air temperature, and Q is the applied heat load. This metric provides an additional measure of cooling effectiveness because lower thermal resistance indicates more effective heat removal from the MMIC to the surrounding airflow.

3.9. Numerical Reliability and Limitations

Although experimental validation is not included in the present study, numerical reliability is supported through the grid-independence analysis, consistent solver settings across all simulated configurations, and physically consistent thermal trends observed with changes in airflow organization and heat-sink integration. The predicted trends also agree with established forced-air electronics cooling behavior, where airflow path organization, reduction of recirculation zones, and increased convective surface area are known to improve cooling effectiveness [8,15–18,21].

Accordingly, the present methodology should be interpreted primarily as a comparative system-level optimization framework. The emphasis is placed on identifying robust thermal-design trends and practical engineering guidance rather than on claiming exact prediction of absolute device junction temperature. The reported temperatures therefore represent comparative maximum MMIC surface temperatures under the specified simulation assumptions and boundary conditions.

4. Results and Discussion

4.1. Baseline Thermal Performance

The baseline configuration consists of the GaN MMIC mounted on a copper heat spreader inside an aluminum enclosure and cooled using the initial vertical forced-airflow arrangement. Under the specified device heat load of 42 W and an ambient inlet air temperature of 25 °C, the predicted maximum MMIC surface temperature reaches approximately 50 °C.

The temperature distribution for this configuration is shown in Fig. 5. The highest-temperature region is concentrated near the center of the copper base directly beneath the MMIC. This localized hot spot corresponds to the primary heat-generation region and indicates that the baseline cooling arrangement provides limited heat spreading and nonuniform convective heat removal.

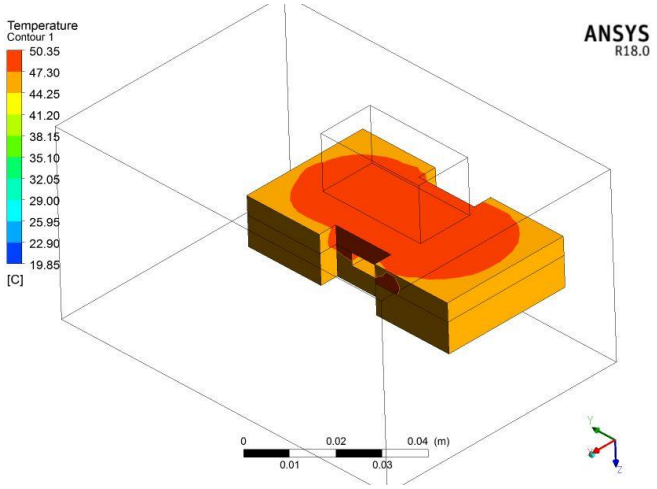

Fig 5. Temperature distribution of the baseline cooling configuration under vertical airflow, showing a peak MMIC surface temperature of approximately 50 °C.

The corresponding airflow streamlines, illustrated in Fig. 6, show nonuniform flow distribution inside the enclosure. Recirculation zones are observed near the enclosure walls, and airflow penetration toward the thermally critical MMIC region is limited. As a result, convective heat removal is not fully utilized, leading to elevated maximum temperature and reduced thermal uniformity.

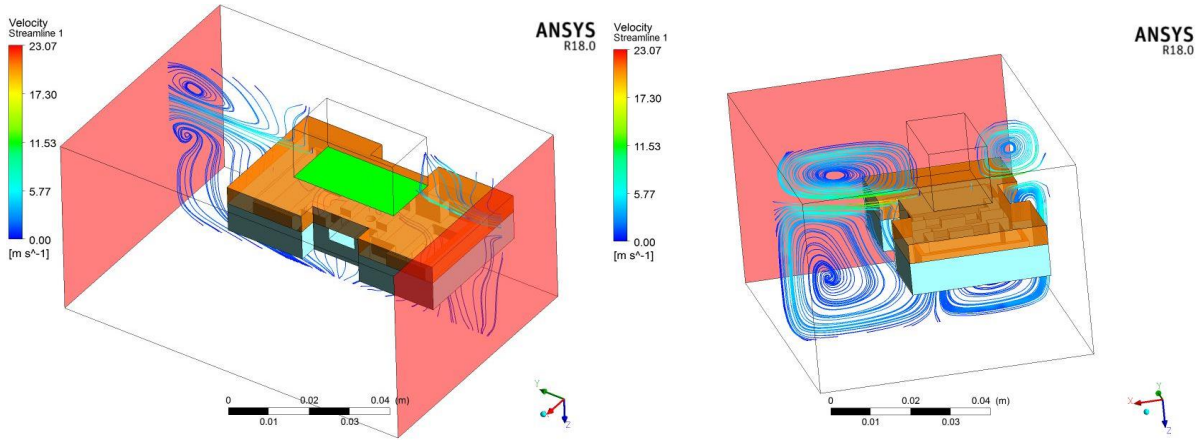

(a) (b)

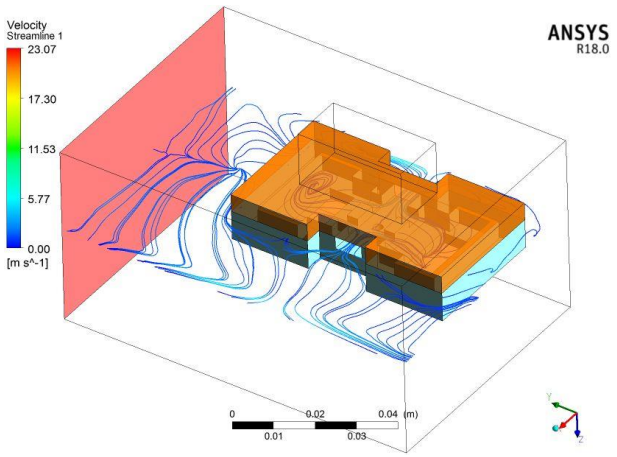

(c)

Fig 6. Airflow streamlines for the baseline configuration in three orthogonal planes: (a) Y–Z plane, (b) X–Z plane, and (c) X–Y plane.

These results establish the thermal limitation of the original cooling configuration and provide a reference for evaluating the effectiveness of the subsequent design modifications.

4.2. Effect of Fan-Performance Enhancement

To improve convective heat removal, the baseline fan condition was replaced by a higher-capacity fan condition while maintaining the same enclosure geometry, fan/inlet position, outlet position, airflow direction, heat load, and material properties. Therefore, the fan-performance enhancement case isolates the influence of increased airflow capacity without changing the airflow path or physical layout of the enclosure.

This modification reduced the predicted maximum MMIC surface temperature from approximately 50 °C to approximately 43 °C, corresponding to a temperature reduction of about 7 °C relative to the baseline case. The temperature contours shown in Fig. 7 indicate improved thermal distribution across the copper base and surrounding enclosure components. This improvement is attributed to the increased airflow capacity, which enhances convective heat removal from exposed heated surfaces.

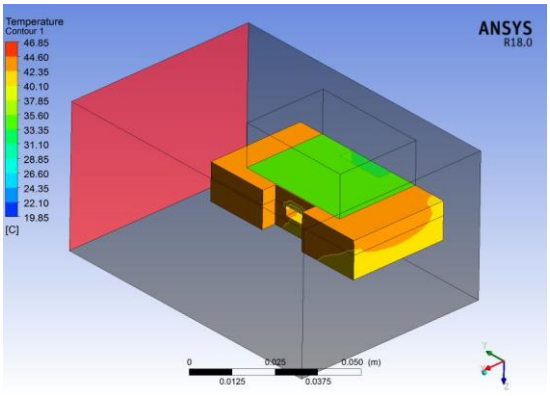

Fig 7. Temperature distribution of the cooling system with fan-performance enhancement, showing reduced peak surface temperature relative to the baseline case.

However, despite the reduction in maximum temperature, the fan-enhancement case does not fully eliminate the airflow nonuniformity observed in the baseline configuration. Local recirculation and stagnant regions remain inside the enclosure because the direction of the airflow path is unchanged. This indicates that increasing fan capacity alone is helpful but insufficient for achieving the best cooling performance in a compact enclosure. Airflow organization and flow-path design must also be considered.

4.3. Effect of Airflow Re-Orientation

To address the limitations of the vertical airflow arrangement, the inlet and outlet organization was modified to promote lateral airflow across the heat-dissipating components. Unlike the fan-performance enhancement case, this modification changes the direction of airflow interaction with the MMIC, copper heat spreader, and enclosure surfaces.

As shown in Figs. 8–10, the lateral airflow configuration produces a more organized flow path across the thermally active region. The airflow is directed more effectively over the MMIC and copper base, improving convective heat transfer and reducing localized stagnant zones. This modification decreases the maximum MMIC surface temperature to approximately 39 °C, corresponding to an 11 °C reduction relative to the baseline configuration.

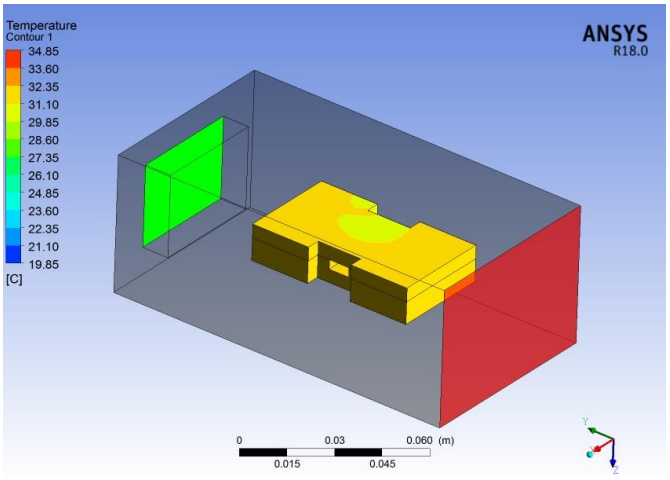

Fig 8. Temperature distribution for the lateral airflow configuration, showing reduced peak MMIC surface temperature compared with the vertical airflow case.

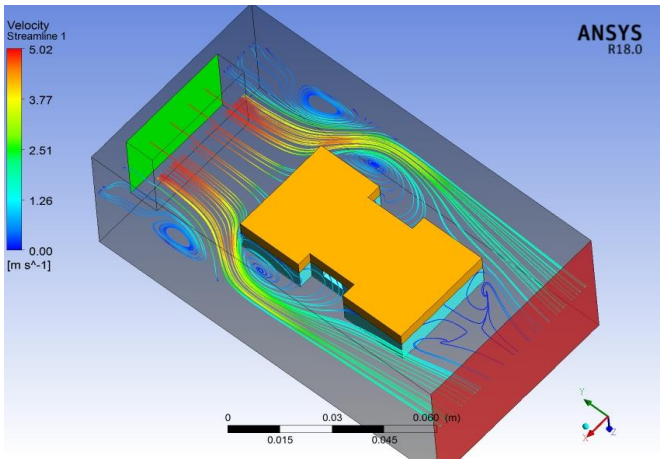

Fig 9. Vortex structures formed inside the enclosure under lateral airflow conditions.

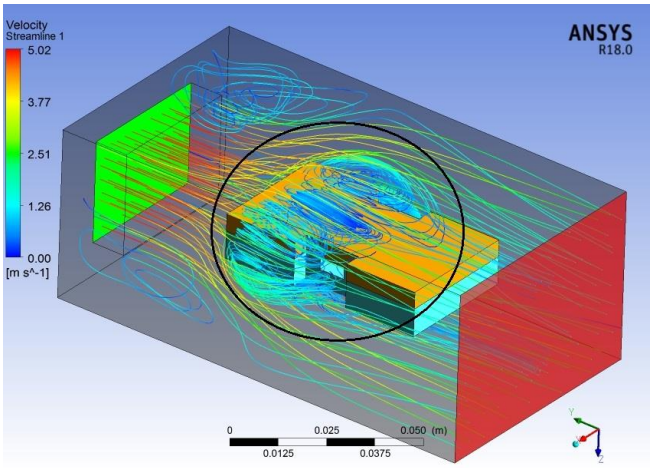

Fig 10. Airflow streamlines and velocity vectors for the lateral airflow configuration.

The results demonstrate that airflow direction and enclosure flow organization strongly influence cooling effectiveness. Compared with simply increasing fan capacity, airflow re-orientation provides a larger thermal benefit because it improves the interaction between the moving air and the heat-dissipating surfaces.

4.4. Effect of Heat-Sink Integration

After improving the airflow organization, a compact finned copper heat sink was integrated into the lateral airflow path. The purpose of the heat sink is to increase the effective convective surface area and improve conductive heat spreading from the MMIC region to the surrounding airflow.

The optimized heat-sink-integrated configuration is shown in Figs. 11–15. In this configuration, the lateral airflow passes through or across the finned heat-sink region, increasing the air–solid contact area and improving thermal interaction between the airflow and the heat-dissipating structure.

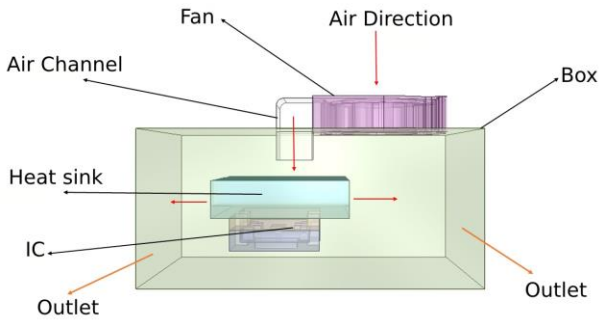

Fig 11. Optimized cooling configuration with integrated air channel and finned copper heat sink.

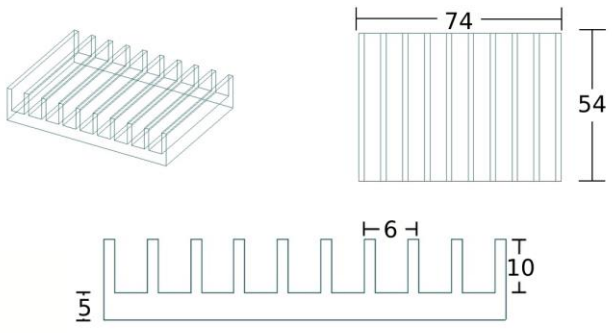

Fig 12. Geometry and dimensions of the finned copper heat sink used in the optimized configuration.

(a)

(b)

Fig 13. Heat-sink integration within the amplifier enclosure: (a) side view and (b) top view.

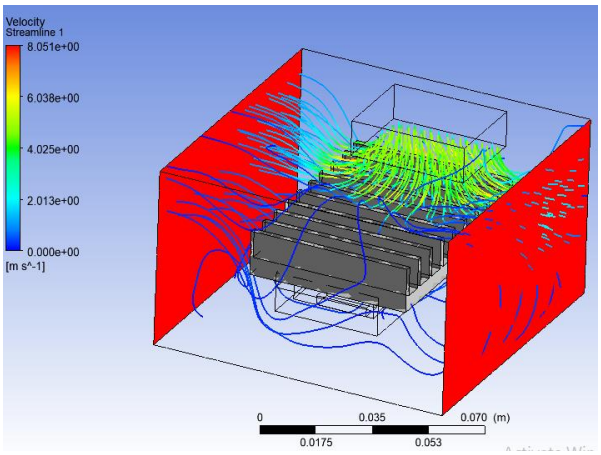

Fig 14. Airflow streamlines and velocity contours around the integrated heat sink.

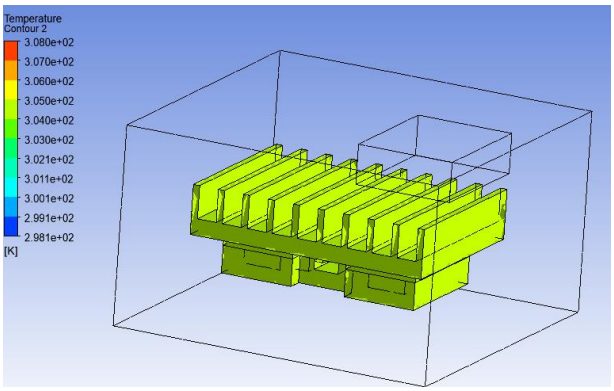

Fig 15. Temperature distribution of the final optimized cooling configuration with lateral airflow and heat-sink integration, showing a peak MMIC surface temperature of approximately 35 °C.

The final heat-sink-integrated configuration provides the largest thermal improvement among the investigated cases. The maximum MMIC surface temperature is reduced to approximately 35 °C, corresponding to a total reduction of approximately 15 °C relative to the baseline configuration.

This improvement is due to the combined effect of enhanced conductive heat spreading through the copper heat sink, increased surface area for convective heat transfer, and improved airflow interaction with the heat-dissipating surfaces. In addition, the temperature distribution becomes more uniform, and the intensity of the localized hot spot is substantially reduced.

4.5. Comparative Thermal Performance and Thermal Resistance

The sequential optimization approach allows the thermal contribution of each design modification to be compared systematically. Tab. 4 summarizes the maximum MMIC surface temperature, temperature reduction, relative improvement, and estimated thermal resistance for each investigated configuration.

The thermal resistance is calculated using Eq. (8), based on the maximum MMIC surface temperature, ambient inlet air temperature, and applied heat load. In this study, the ambient inlet air temperature is 25 °C and the applied heat load is 42 W.

Table 4. Comparative thermal performance and estimated thermal resistance of the investigated configurations

Configuration	Max Temperature (°C)	Temperature Reduction (°C)	Relative Improvement (%)	Thermal Resistance, R_{th} (K/W)
Baseline configuration	50.0	—	—	0.595
Fan-performance enhancement	43.0	7.0	14.0	0.429
Airflow re-orientation	39.0	11.0	22.0	0.333
Heat-sink-integrated optimized configuration	35.0	15.0	30.0	0.238

The results show a clear and progressive improvement in cooling performance across the investigated configurations. The baseline case has the highest thermal resistance, 0.595 K/W, indicating the least effective heat removal. Increasing fan capacity reduces the thermal resistance to 0.429 K/W, confirming that higher airflow capacity improves convective heat removal. However, the airflow re-orientation case further reduces the thermal resistance to 0.333 K/W, demonstrating that airflow-path organization can provide greater thermal benefit than fan-capacity increase alone.

The final heat-sink-integrated configuration achieves the lowest thermal resistance, 0.238 K/W. This confirms that the combined use of lateral airflow organization and passive heat-sink integration provides the most effective thermal-management strategy among the investigated cases. Therefore, Eq. (8) is retained because it provides an additional quantitative measure of cooling effectiveness beyond maximum temperature reduction alone.

4.6. Engineering Implications

The results indicate that thermal optimization of compact GaN MMIC amplifier systems should not rely only on increasing fan capacity. Although a higher-capacity fan improves cooling performance, the larger improvement is achieved when the airflow path is organized to interact more effectively with the thermally critical regions.

From a practical design perspective, the following design sequence is recommended:

- improve airflow path and inlet/outlet organization to reduce recirculation and stagnant zones;
- direct airflow across the MMIC, copper heat spreader, and other heat-dissipating surfaces;
- integrate compact passive thermal structures, such as finned copper heat sinks, to increase heat-transfer area;
- increase fan capacity only after airflow-path organization has been considered.

This approach is especially relevant for compact RF and microwave electronic systems where enclosure volume is limited, liquid cooling is impractical, and cost, simplicity, and scalability are important design constraints.

The final heat-sink-integrated lateral airflow configuration should therefore be interpreted as the best-performing configuration among the investigated design cases, rather than as a global optimum over all possible fan positions and enclosure layouts. This distinction is important because the present study focuses on a practical sequential optimization strategy for engineering design improvement.

5. Conclusion

This study presented a system-level thermal optimization framework for improving the forced-air cooling performance of a compact high-power GaN MMIC amplifier under enclosure-level design constraints. A three-dimensional conjugate heat-transfer numerical model was used to evaluate the coupled effects of heat conduction in the solid components and forced convection within the internal airflow region. The investigated cooling configurations included the baseline vertical airflow arrangement, fan-performance enhancement, airflow re-orientation, and lateral airflow combined with a compact finned copper heat sink.

The results demonstrate that airflow organization plays a critical role in the thermal behavior of compact electronic systems. Increasing the fan capacity reduced the maximum MMIC surface temperature from approximately 50 °C to 43 °C; however, local recirculation and nonuniform airflow remained because the airflow path was unchanged. Re-orienting the airflow laterally across the MMIC and copper heat spreader further reduced the maximum temperature to approximately 39 °C by improving airflow interaction with the thermally critical region.

The best-performing configuration among the investigated cases was obtained by combining lateral airflow organization with a compact finned copper heat sink. This configuration reduced the maximum MMIC surface temperature to approximately 35 °C, corresponding to an overall temperature reduction of about 15 °C relative to the baseline case. The estimated thermal resistance also decreased progressively across the optimization stages, confirming that the combined use of improved airflow path organization and passive heat-sink integration provides the most effective thermal-management strategy among the studied configurations.

The findings suggest that effective thermal design for compact GaN MMIC amplifier systems should prioritize airflow-path management and passive heat-spreading enhancement before relying solely on increased fan capacity. This approach is especially relevant for compact RF and microwave electronic systems where space, cost, simplicity, and scalability are important design constraints.

It should be noted that the term “optimized configuration” in this study refers to the best-performing configuration among the sequentially investigated design modifications, rather than a global mathematical optimization over all possible fan positions, inlet/outlet arrangements, and heat-sink geometries. In addition, the present work is limited to steady-state numerical analysis and does not include experimental validation. Future work will focus on experimental temperature measurements, transient thermal behavior, detailed fan-curve characterization, and extension of the methodology to higher power-density GaN devices and more advanced packaging configurations.

Acknowledgment

The authors gratefully acknowledge the support of the Robotic Century Innovation Laboratory for providing computational resources and technical discussions that contributed to this research.

References

[1] Mishra, U. K., et al., AlGaN/GaN HEMTs—An Overview of Device Operation and Applications, *Proceedings of the IEEE*, 90 (2002), 6, pp. 1022-1031

[2] Palacios, T., et al., High-Power AlGaN/GaN HEMTs for RF Applications, *IEEE Transactions on Microwave Theory and Techniques*, 53 (2005), 3, pp. 1250-1258

[3] Chowdhury, S., Mishra, U. K., Lateral and Vertical Transistors Using the AlGaN/GaN Heterostructure, *IEEE Transactions on Electron Devices*, 60 (2013), 10, pp. 3060-3066

[4] Sheppard, S. T., et al., High Thermal Conductivity Substrates for GaN Power Devices, *IEEE Electron Device Letters*, 30 (2009), 4, pp. 288-290

[5] Meneghini, M., et al., Reliability of GaN High-Electron-Mobility Transistors: State of the Art and Perspectives, *IEEE Transactions on Device and Materials Reliability*, 16 (2016), 3, pp. 525-544

[6] Timoshenkov, S. P., et al., Numerical Thermal Analysis of C-Band GaN Power Transistors under Pulsed Operation, *Microelectronics Reliability*, 100 (2019), 113392

[7] Chu, R. M., et al., Overview of Advanced Cooling Technologies for Power Electronics, *Applied Thermal Engineering*, 127 (2017), pp. 308-326

[8] Patil, A., Chavan, S., 3D Thermal Modeling and Optimization of High-Power IC Chips under Forced Convection, *Thermal Science and Engineering Progress*, 24 (2021), 100915

[9] Goyal, N., Kumar, M., Self-Healing Circuit Architecture for Thermal Reliability in 3D Integrated Systems, *Microelectronics Reliability*, 114 (2020), 113771

[10] Zhuo, R., et al., Microchannel Cooling Design for High-Frequency MMIC and Antenna Systems, *Applied Thermal Engineering*, 148 (2019), pp. 1061-1070

[11] Gupta, A., Kumar, V., Low-Temperature Co-Fired Ceramic Packaging for High-Frequency Microwave Applications, *Journal of Electronic Packaging*, 142 (2020), 3, 031004

[12] Sundaram, V., et al., Thermal-Performance Enhancement in Laminate and Glass Fan-Out Packaging for Power Amplifiers, *IEEE Transactions on Components, Packaging and Manufacturing Technology*, 11 (2021), 2, pp. 286-295

[13] Lee, Y., et al., Air-Cooled Metal Microchannels for High Heat-Flux Microelectronic Applications, *International Journal of Heat and Mass Transfer*, 184 (2022), 122274

[14] Pozar, D. M., *Microwave Engineering*, 4th ed., Wiley, Hoboken, NJ, USA, 2011

[15] Çengel, Y. A., Ghajar, A. J., *Heat and Mass Transfer: Fundamentals and Applications*, 5th ed., McGraw-Hill, New York, USA, 2015

[16] Versteeg, H. K., Malalasekera, W., *An Introduction to Computational Fluid Dynamics: The Finite Volume Method*, 2nd ed., Pearson Education, Harlow, UK, 2007

[17] Incropera, F. P., DeWitt, D. P., *Fundamentals of Heat and Mass Transfer*, 5th ed., Wiley, New York, USA, 2002

[18] ***, *ANSYS Fluent Theory Guide*, Release 2023, ANSYS Inc., Canonsburg, PA, USA, 2023

[19] Lasance, C. J. M., Ten Years of Boundary-Condition-Independent Compact Thermal Modeling of Electronic Parts: A Review, *Heat Transfer Engineering*, 29 (2008), 2, pp. 149-168

[20] Jebelli, A., et al., Enhancing Efficiency and Reliability in High-Power Microwave Amplifiers: A Novel Circuit Driver Approach, *International Journal of Robotics and Automation*, 14 (2025), 1, pp. 82-92

[21] Jebelli, A., et al., Advanced Thermal Management for High-Power ICs: Optimizing Heatsink and Airflow Design, *Applied Sciences*, 14 (2024), 20, pp. 1-14

[22] ***, *QPA1010: 7.9-11.0 GHz 15 W GaN Power Amplifier Data Sheet*, Rev. J, Qorvo Inc., Greensboro, NC, USA, 2025

Paper submitted: 04 April 2026

Paper revised: 18 May 2026

Paper accepted: 25 May 2026